Tectonophysics 856 (2023) 229849

Contents lists available at ScienceDirect

Tectonophysics

journal homepage: www.elsevier.com/locate/tecto

Microseismicity clustering and mechanic properties reveal fault segmentation in southern Italy

Mauro Palo *, Matteo Picozzi, Grazia De Landro, Aldo Zollo

Physics Department 'Ettore Pancini', University of Naples Federico II, Complesso Universitario di Monte Sant'Angelo – Via Cinthia, 21, 80126 Napoli, Italy

ARTICLE INFO

Keywords:
Microseismicity
Clustering
Fault segmentation
Normal faulting
Irpinia

ABSTRACT

We analyze the clustered microseismicity recorded over more than one decade in the Irpinia region, an active seismic area in Southern Italy. We studied the spatiotemporal properties of rate, source parameters and slipping mechanisms of the clustered seismicity in relationship with local medium properties and the deformation signal. Spatial pattern of both medium properties and source parameters indicates a segmentation along strike of the fault network with evidence of a high- and a low-coupling segments separated by a region with diffused microseismicity and high b-value. The high-coupling segment shows high fraction of clustered seismicity, low b-value, high relative coseismic slip, low Vp/Vs (1.7–1.75) and near-repeating earthquakes. We find that the seismicity in this high-coupling segment is triggered by non-tectonic loading, such as the recharge of a karst aquifer, suggesting a system close to critical conditions. The high-coupling segment can be identified as a potential strong motion area for future earthquakes, while the intermediate segment can mark the edges of an extensional transfer zone, which can act as a discontinuity for slip propagation. The low-coupling segment is the same where the Ms. 6.9, 1980 Irpinia earthquake nucleated. This segment shows today both relatively high b-values and high coseismic slip, but above all it shows temporal dependencies in its properties, which leads us to pay attention to it for the future spatiotemporal evolution of microseismicity in this area.

1. Introduction

Frictional and mechanical properties of the faults rule the accommodation of the tectonic loading and eventually determine where and when an earthquake nucleate and to which extent the fracture propagates along the interface (e.g., Lay and Kanamori, 1981; Lay et al., 2012; Niemeijer and Vissers, 2014). Many observations in the last decades have shown that frictional properties can sharply change both along strike and depth leading to the definition of fault interface domains with peculiar frictional regimes and coupling (Bilek and Lay, 2002; Johnson, 2006; Moreno et al., 2012; Avouac, 2015). Such faults segmentation finds its origin in their long-term history ('structural maturity') and geometry (Manighetti et al., 2007).

Italy is one of the most seismically hazardous countries in the Mediterranean region. Despite the worst historical earthquakes along the Apennine chain in Italy were all characterized by magnitude between 6 and 7 (i.e., the 1908 Mw 7.0 Messina earthquake; the 1915 Mw 6.7 Fucino earthquake; the 1980 Ms. 6.9 Irpinia earthquake; the 2009 Mw 6.1 L'Aquila earthquake; and the 2016 Mw 6.5 Norcia earthquake), >120,000 people were killed by earthquakes during the last century (Valensise and Pantosti, 2001). A peculiar feature of large earthquakes in Italy is of being followed within seconds to months by large aftershocks of magnitude like the initial quake or even larger, demonstrating the complexity of the Apennines' faults system (Gentili and Di Giovambattista, 2017). Such mechanical behavior of faults finds its origin in the alternation of compressional and extensional regimes during the Apennines buildup phases (Barchi, 1998). Recent seismicity in the Apennines highlighted that segmentation and the complex evolution of the rupture are related to the interference of normal faults with preexisting thrust structures (Chiarabba and Amato, 2003). In this framework, a crucial role is also played by crustal fluids. Indeed, the large shocks of the 2016 central Italy seismic sequence were likely triggered by high pore pressure at the footwall (Chiarabba et al., 2018). Recent studies hypothesize a dominant role for high crustal fluid pressure as triggering mechanism for the nucleation of large earthquakes in pre-existing faults in the Apennines in several cases, which in turn leads to the activation of other closely spaced fault segments (Di Luccio et al., 2010; Doglioni et al., 2014).

* Corresponding author.
E-mail address: mauro.palo@unina.it (M. Palo).

https://doi.org/10.1016/j.tecto.2023.229849
Received 15 November 2022; Received in revised form 18 February 2023; Accepted 5 April 2023
Available online 20 April 2023

Unveiling the segmentation and the complex interaction between adjacent faults during the interseismic period becomes a crucial goal with important implications for seismic hazard. The seismological community is thus seeking for new tools to achieve a better understanding of crustal strength without waiting for the final stages of the processes that lead to the rupture. A possible means way to achieve these goals is the analysis of the spatiotemporal evolution of small magnitude earthquakes (hereinafter, microseismicity), which can improve our understanding of fault structures and mechanical properties, and to capture any preparatory process that anticipates large earthquakes as well (Picozzi et al., 2022c, 2022d). In particular, the spatiotemporal clustering of microseismicity can provide insights on the accumulation and transfer of tectonic stress and can be considered a proxy of the local coupling conditions over the fault interface (Liu et al., 2022). Long-term monitoring of the microseismicity can thus provide information on both the small-scale mechanical properties of rocks hosting the faults and their evolution (Amoroso et al., 2017; Doetsch et al., 2018; De Landro et al., 2022; Herrmann et al., 2022) and on the earthquake rupture dynamics through the inversion of seismic data (Wang et al., 2019; Picozzi et al., 2022a).

Here, we investigate the potential of microseismicity in characterizing a complex set of faults responsible for the 1980, Ms. 6.9 Irpinia earthquake in southern Italy (hereafter 1980 EQ); the latter was a pure normal-faulting event characterized by cascading rupture episodes occurred at 10, 18, and 39 s after the first shock, which in total activated four different faults: Marzano, Cervialto, San Gregorio and Conza (Bernard and Zollo, 1989; Pantosti and Valensise, 1990) (see Fig. 1). The Irpinia earthquake caused about 3000 fatalities and severe damage, which stimulated the development of the Irpinia Near Fault Observatory (INFO, https://www.epos-eu.org/tcs/near-fault-observatories).

Studying the microseismicity in the Irpinia region and its spatio-temporal clustering properties can be relevant for understanding key features of the fault segmentation and the generation of large earthquakes in extensional context (Festa et al., 2021; Picozzi et al., 2022a, 2022b). The recent seismicity in the area appears: i) mostly confined within the same volume where the mainshock of 1980 EQ and its aftershocks were located, but the long time passed from such mainshock let us be confident of studying the faults within an interseismic period; ii) This area is monitored since 2005 by the Irpinia Seismic Network (ISNet, Weber et al. (2007); Iannaccone et al. (2010)) made of 31 stations, which in the framework of the EPOS has developed into a Near Fault Observatory (NFO). The ISNet network thus represents a real-world seismological laboratory. iii) source parameters and ground motion intensity show temporal variation and a heterogenous spatial distribution suggesting faults with different mechanical properties (Picozzi et al., 2019; Picozzi et al., 2022a, 2022b). iv) The background seismicity is modelled to be controlled by high pore fluid pressure, whereas an intensely fractured damage zone of main faults, where currently microseismicity concentrates, acts as conduit system allowing fluid circulation (Amoroso et al., 2014). v) A tight interconnection has been

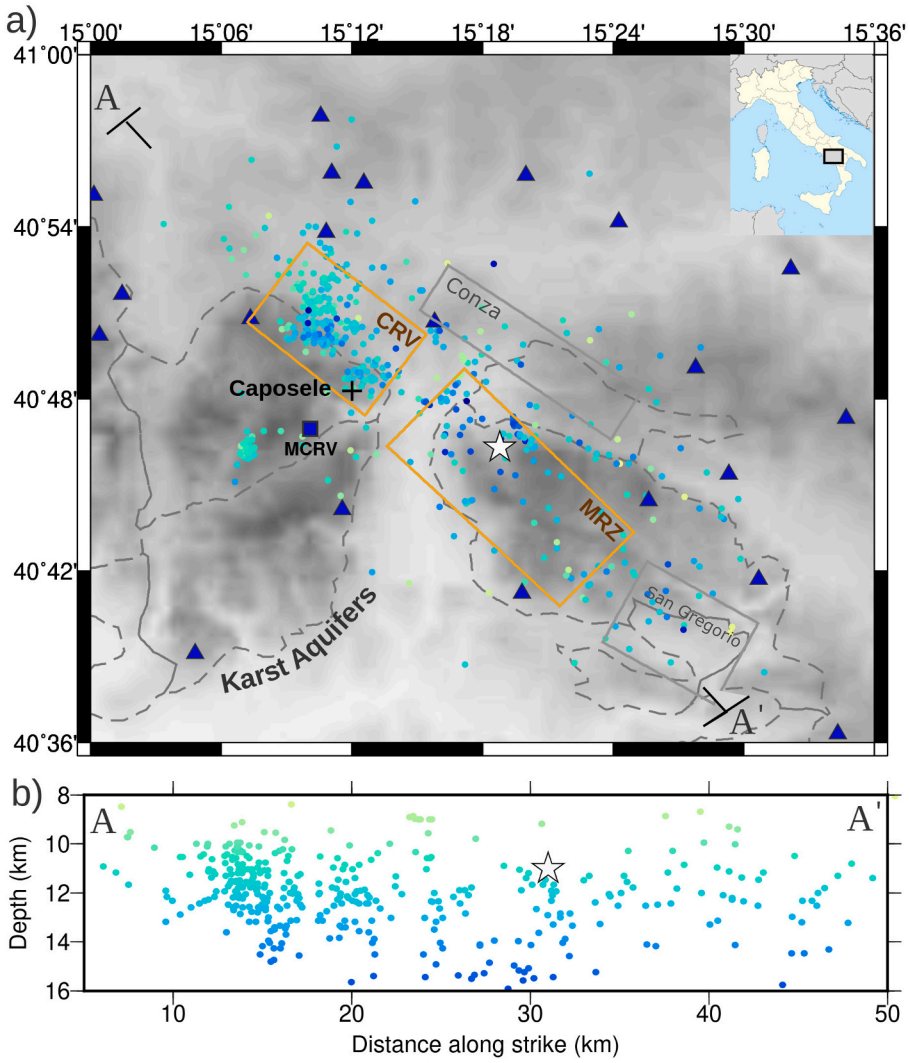

Fig. 1. Tectonic setting of the Irpinia Fault System. (a) Geological sketch map. The orange and gray boxes are the Irpinia Faults as reported by Pantosti and Valensise (1993). The two orange boxes correspond to the Cervialto (CRV) and to the Marzano (MRZ) fault segments considered in this study. The gray dashed contoured areas represent the Apennines carbonate rocks. The grayscale represents the topographic map. The blue triangles are the ISNet stations and the blue square is the MCRV geodetic station. The circles indicate the events used in this study that are coloured according to their depth. The black cross represents the Caposele spring. (b) Distribution of seismicity in cross-section along longitude. In both subplots the white star marks the hypocenter of the 1980 EQ. (For interpretation of the references to colour in this figure legend, the reader is referred to the web version of this article.)

observed also between groundwater recharge of karst aquifers and background seismicity (D'Agostino et al., 2018), suggesting that external forcing can induce pulsating, pore pressure changes at depths where large earthquakes nucleate (i.e., 10–12 km, De Landro et al., 2022).

These aspects made the Irpinia area an ideal setting for investigating how microseismicity can contribute to unveil the segmentation and the complex interaction between adjacent faults and enlighten the complex fault network and their stress conditions in a region potentially able to generate a M7 earthquake.

2. Dataset

We analyze the microseismicity (M < 3.5) of the Irpinia area from February 2008 to March 2020 recorded by ISNet and reported in the seismic bulletin. Among this seismicity, we extract the earthquakes broadly located in the volumes of the two fault segments of Cervialto and Marzano (marked with orange lines in Fig. 1a). We select for this area the seismicity between 8 km and 15 km of depth that corresponds to the range where large magnitude earthquakes nucleate. In this way, the final catalog consists of 487 earthquakes with magnitude (Mw) ranging in the interval 1–3.2. Hypocentres of the selected events were obtained by De Landro et al. (2022) inverting manually picked P and S arrivals times with a nonlinear location method (NLLoc, Lomax et al., 2009) in 3D P- and S-wave velocity models optimized for the area.

The volume embedding the fault segments of Cervialto and Marzano was activated during the first rupture episode of the 1980 EQ. A large co-seismic slip was recorded on these segments during the mainshock of the 1980 EQ, while the "Sele plain", that separates the two segments, was nearly aseismic during the event (Bernard and Zollo, 1989). Currently Marzano and Cervialto segments host most of the local microseismicity (Picozzi et al., 2022a).

3. Methods

We look for families of earthquakes sharing similar waveforms (hereafter clusters) by a new clustering approach (hereafter multi-channel clustering, or shortly MCC) based on the Hierarchical Agglomerative Clustering (HAC) applied to the cross-correlation (CC) matrix built pairwise on the signals of the earthquakes. Similarly to other applications (e.g., Rowe et al., 2002; Shearer et al., 2005; Hotovec-Ellis and Jeffries, 2016; Trugman and Shearer, 2017), MCC starts from the calculation of the one-station CC matrices built with the pairs of earthquakes recorded at one station. Here, we form these matrices using the P phase. The similarity between a pair of earthquakes *i,j* can be thus measured either using CC_{ij} at a reference station (that detects, for example, the largest number of earthquakes of the catalog) or evaluating a statistics (e.g., the average or the median) of the CC_{ij} at different stations. This step is included also in MCC, where we use as statistic parameter the largest CC_{ij} over the stations. However, this step implies that potentially a cluster index can be assigned only to a subset of the catalog. Moreover, if two earthquakes are not detected at any common station, a measure of their similarity is not possible. Nevertheless, the MCC approach is able to overcome this issue, and an estimate of the similarity for such cases is provided. We implement the method as follows: we first define one-station clusters of signals sharing similar waveforms. Then, we consider signals belonging to the same one-station cluster of an earthquake not detected at a given station as a good representation of it. In this framework, if a pair of earthquakes *i,j* is not detected at any common station, we search for stations detecting one or more earthquakes of their one-station clusters, calculate the CC between them and properly combine the results to get an estimate of the similarity between the earthquake pair *i,j*. In the end, in MCC a matrix describing the similarity between all pairs of earthquakes of the catalog is built. We finally apply HAC to MCC to assign a cluster label to each earthquake. An extensive description of the algorithm and all numerical details are provided in Appendix.

The cluster indexing from MCC therefore: 1. does not depend on a specific station chosen for CC calculation – in that sense, MCC assigns a cluster index to the "source" of the earthquake and not to its recordings at one station; 2. combining single- and multi-station clustering, can be more accurate and complete in defining families of earthquakes and less sensitive to fictitious signal similarities at individual stations (due for example to strong site effects).

We remark that MCM assigns a cluster label to the earthquakes of an already defined catalog, and no new earthquakes are detected by this technique, differently from other approaches that aim to enlarge the earthquake catalog and that, using the fingerprints of an earthquake as a template, look for similar samples and build therefore families of previously unknown events (e.g., Shelly et al., 2016).

Among all clusters found by MCC, we select only those with high CC values (see Appendix) to isolate the earthquakes that can be considered as generated by multiple activations of common or close faults. We define these selected clusters as forming the clustered seismicity, whereas the rest of seismicity is defined as background. Out of the 487 earthquakes of the catalog, 143 events belong to the clustered seismicity (see Supplemental Material for the catalog of the clustered seismicity). Interestingly, Marzano and Cervialto segments show very different fractions of clustered seismicity, respectively about 10% and 44%. In Fig. 2 the occurrence times of the events of each selected cluster are plotted together with an example of the waveforms of a cluster. An index has been assigned to each cluster; it ranges between 1 and 20 and increases moving from NW to SE.

As reconstructing with high accuracy the cluster patterns is crucial to confirm the proximity of the events and to detect repeating earthquakes, earthquakes of the clustered seismicity are relocated with the double-difference (DD) approach by the hypoDD code (Waldhauser and Ellsworth, 2000). Being based on the high-precision differential arrival times of pairs of earthquakes of one cluster, the DD approach can provide a small-scale imaging of the rupture faults.

The differential P and S arrival times between event pairs of the same cluster are computed by maximizing the CC function, which is calculated respectively for P and S phase in a time window between −0.3 s and + 0.5 s with respect to the manually picked P arrival, and between −0.5 s and + 0.7 s with respect to the theoretical S arrival time predicted by the 3D velocity model.

In both cases, the signals are tapered with a Tukey window (alpha factor: 0.4) to minimize inconsistent alignments. We use the differential arrival times when the CC is higher than 0.5, weighting the data based on the CC value. For the application of the DD location method, we use the 1-D velocity model of Matrullo et al. (2013), optimized for the Irpinia area. Hypocenters are updated for 10 iterations. In the first half of the iterations, all available differential arrival times within each cluster are used to constrain the relative locations at a large scale (>1 km). In the latter half of the iterations, we select CC solutions with higher accuracy (CC ≥0.8) for event pairs within 1 km, to delineate small-scale (<1 km) structures of each cluster.

The rms of final locations are lower than 0.05 s for most of the events (Fig. S5a). To have a reliable evaluation of location errors, we compute the Posterior Density Function (PDF, an example is in Fig. S6) of each event with the NLDiffLoc code (De Landro et al., 2015), which performs a global exploration of location parameters in a probabilistic framework by using CC differential times, allowing the use of 3D velocity models. We use the 3D velocity models of De Landro et al. (2015). We find that the location errors inferred from the PDF (with a level of confidence of 68%) are lower than 60 m for most of the seismicity (Fig. S5).

Hypocenters of the DD-relocated earthquakes are plotted in Fig. 3. In the main subplot, the centroid of the cluster is plotted on the plane if the inter-earthquake spacing within a cluster after relocation is similar or lower than the marker size. Each cluster in Fig. 3 is labelled with the corresponding cluster index.

Clustered seismicity is not limited to a specific depth, but similarly to

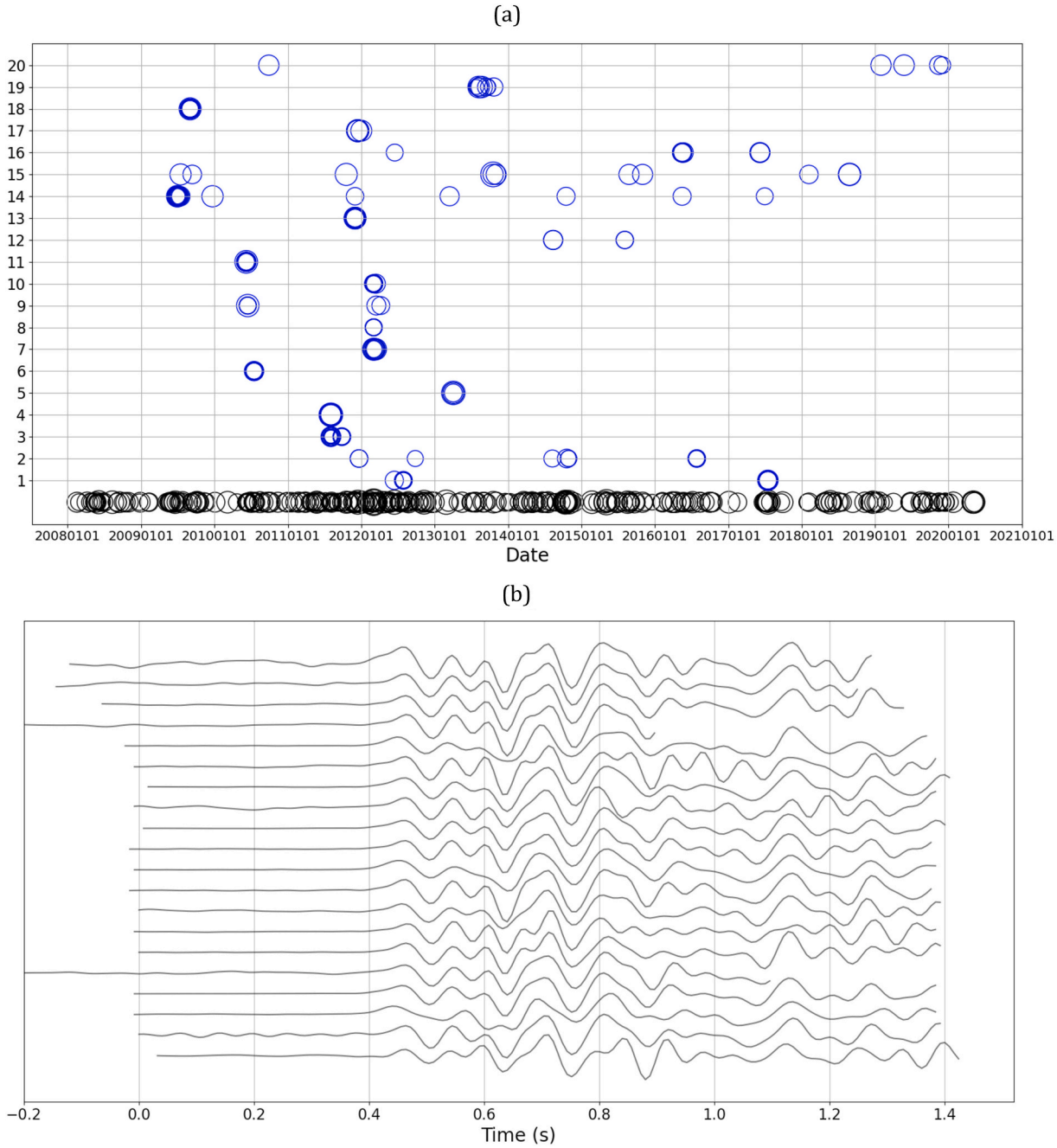

Fig. 2. (a) Time occurrences of the families of earthquakes belonging to the clustered seismicity (blue) and to the background seismicity (black). Cluster index increases moving along the NW-SE profile. Size of the marker scales with Mw. (b) Example of the waveforms of one family of the clustered seismicity (cluster 14) recorded at one station. (For interpretation of the references to colour in this figure legend, the reader is referred to the web version of this article.)

the background, it is spread in the range between 10 km and 15 km. Most of the clusters are located in the south-western half of the slipping area of the 1980 EQ on the Cervialto segment, and the density of the clustered seismicity decreases when moving along the line of the Apennines chain in the SE direction (Fig. 3). Along the anti-Apennines direction, we can identify a gap of about 2 km between the clusters on the Cervialto segment and the others (Fig. S1).

Few clusters appear outside the Cervialto fault segment: two at the southern and northern border of Cervialto and Marzano segments, respectively, and two very close to the hypocenter of the 1980 EQ. Moreover, along the NW-SE profile two main disjoined along-strike segments can be distinguished on the Cervialto segment. These two segments host the groups of clusters 1–11 and 12–16, respectively, and are marked on Fig. 3 as the domains C1 and C2. Interestingly, most of the clusters that nucleate in C2 span over several years, showing thus the characteristics of repeating earthquakes (Uchida and Bürgmann, 2019). On the contrary, in C1 the clusters occur as mainshock-aftershock sequences. The clusters in C2 show on average a larger dispersion of the hypocentres than in C1. This evidence, together with the definition of clusters limited to the similarity of the P phase, suggests referring to them as “near-repeaters” clusters (Vuan et al., 2018).

To better characterize the clusters that nucleate on common faults, we calculate the composite focal mechanisms (CFM) for each cluster by the software FPFIT (Reasenberg, 1985). We use as input the P and S polarities of all earthquakes belonging to a cluster. By doing so, we assume that all earthquakes of one cluster are generated by the same

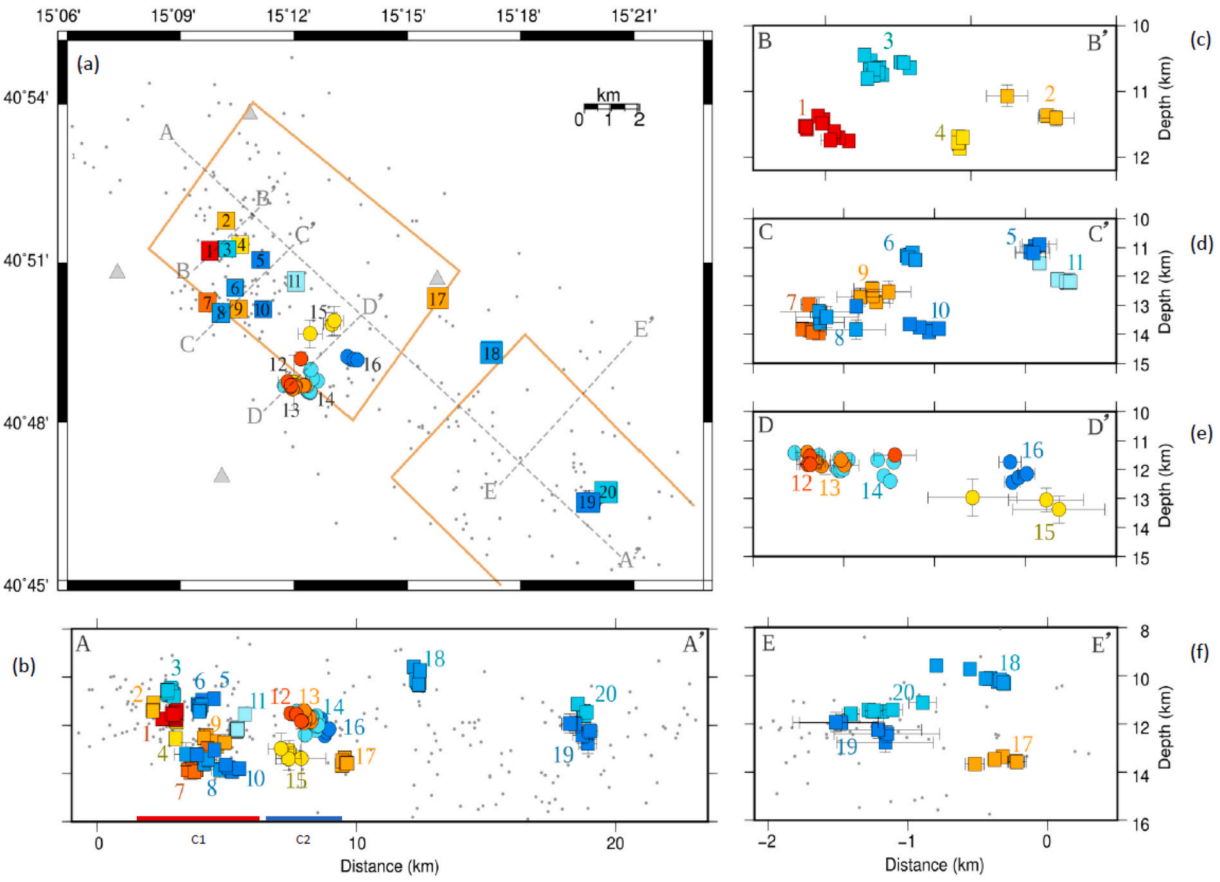

Fig. 3. Spatial distribution of clusters after double-difference re-location. Events with inconsistent differential P and S arrival times are discarded. a) Plane distribution of clusters belonging to domains C1 (squares) and C2 (circles) – as shown in panel (b) - coloured according to the cluster subdivision. The numbers are the cluster indices as in Fig. 2. Clusters of C1 are represented as collapsed in their centroid. The boxes represent the Cervialto and Marzano fault segments. The dashed lines are the profiles of sections in panels b-c-d-e-f. (b) NW–SE vertical section of the clusters. Along-strike the domains C1 and C2 have been defined based on the spatial agglomeration of the clusters 1–11 and 12–16, respectively. (c) SW-NE vertical section of the clusters within 1 km from the profile BB' in panel a. (d) SW-NE vertical section of the clusters within 1 km from the profile CC' in panel a. (e) SW-NE vertical section of the clusters within 1 km from the profile DD' in panel a. (f) SW-NE vertical section of the clusters within 6 km from the profile EE' in panel a.

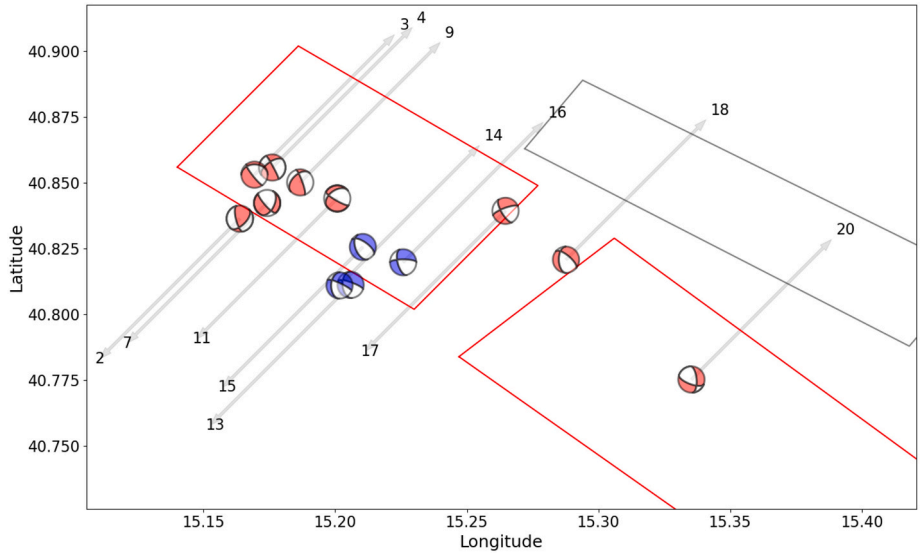

Fig. 4. Composite focal mechanisms corresponding to each family of the clustered seismicity distinguishing sequences (red) and near-repeaters (blue). P and S polarities used for the inversion are extracted from the Isnet bulletin. If the total amount of well-defined polarities for a cluster was lower than 6, no focal mechanism was associated to the cluster. (For interpretation of the references to colour in this figure legend, the reader is referred to the web version of this article.)

slipping mechanism. Hence, we have multiple polarities for each station, which in our framework may be considered as redundant observations of a common source mechanism. In the application of the technique, we use only robust and well-defined readings of polarity.

The alignment in C2 of clusters 12, 13, 14, 16 suggests that they nucleate on a common slipping fault. This is confirmed also by their focal mechanisms, that consistently show a common normal fault mechanism very similar to the fault mechanism found for the mainshock of 1980 EQ (Westaway and Jackson, 1987).

Cluster 15 appears, instead, to be generated on a different, possibly sub-parallel, fault.

Differently, when considering C1, even though earthquakes in this domain mostly show a clear alignment within the single cluster, a pattern defining a common slipping fault is hard to detect. The complexity of this domain is also confirmed by the focal mechanisms, which show a variability of the slip mechanisms ranging from normal faulting to strike slip (Fig. 4). The cluster at the southern boundary of Cervialto segment (cluster 17) shows a nearly pure strike-slip focal mechanism. Differently, the slipping mechanisms generating the events of clusters 18 and 20, respectively located at the northern edge of Marzano segment and close to the hypocenter of 1980 EQ, show both a normal fault component.

The fraction of clustered seismicity over time shows a nearly intermittent behavior, with clustered seismicity disappearing for intervals with low seismicity rate and in general decreasing when the overall seismicity decreases too (Fig. 5).

In Fig. 6a and b, we compare the cluster distributions with the spatial variability of the b-value of the Gutenberg-Richter (GR) law (Gutenberg and Richter, 1942) derived by Picozzi et al. (2022a). The b-value was estimated using the whole-magnitude-range method implemented in the software package ZMAP (Wiemer, 2001) and obtained by the maximum likelihood approach (Aki, 1965). The uncertainty on the b-values was computed by a bootstrap approach (Efron, 2000) and ranges nearly in the interval 10%–30% (see Fig. 8a and S7). More details can be found in the original paper.

We observe that the clustered seismicity preferentially nucleates in areas with relatively low b-values (Fig. 6a-b). In fact, the clustered seismicity that nucleates in the C1-domain spatially matches an area of b-value in the range 0.9–0.95; the latter edges at SE another area with even lower b-values, spatially matching the C2-domain where the b-values range in the interval 0.8–0.9 (Fig. 6). These results are giving insights on a segmentation of the b-value along the Cervialto segment, although the uncertainties in the estimates in this segment does not allow a conclusive interpretation. Moving towards SE from the C2-domain, we see a sharp increase of the b-value (to about 1.1 – Figs. 6ab, 8a). This high-b-value segment, which broadly corresponds along-strike to a region between the southern boundary of the Cervialto segment and the hypocenter of the 1980 EQ hosts clustered seismicity at depths around 10 Km. The C2-domain appears thus to represent the boundary between the low and the high-b-value segments located at the southern edge of the Cervialto fault (Figs. 6a, b, blue dots).

Fig. 6c shows the spatial variation of the stress drop, $\Delta\sigma$, derived by Picozzi et al. (2022a) via a generalized inversion technique (GIT - Castro et al., 1990). In the latter approach, the apparent source spectra derived after having removed the contribution of attenuation and site effects were inverted considering a ω^{γ} source model; then M_0 and f_c were then used to estimate $\Delta\sigma$ according to Brune (1970). More details on the inversion procedure can be retrieved in Picozzi et al. (2017, 2022a). Fig. 6c is obtained averaging $\Delta\sigma$ over 3-km bins along the mean strike of the fault segments and distinguishing among background seismicity, sequences, and near-repeaters. Pictures of the along-strike spatial distribution of $\Delta\sigma$ and its uncertainty for the whole seismicity occurred in Irpinia between the 2007 and 2019 are displayed in Fig. S8a,b. We observe that the clustered seismicity in the C1-domain shows on average lower $\Delta\sigma$ values than those of the background seismicity, which in turn shows on average lower $\Delta\sigma$ than the earthquakes of the C2-domain (Fig. 6c). This is especially true for the earthquakes of the Cervialto segment, where the density of the clustered seismicity is higher, making the statistics more robust.

A segmentation of the frictional properties along strike appears also from the relative slip fraction (RSF, Fig. 8b, red line). RSF is computed starting from the slip (D) of each earthquake using the source parameters estimated by Picozzi et al. (2022a) and using the relation $D = (16/7)^{2/3}(1/\pi)^{1/3}\Delta\sigma^{2/3}/\mu$ between slip and stress drop of Kanamori et al. (2000), with μ shear modulus. Then, the same analysis is repeated considering for all events their M_0, but a constant stress drop equal to the average over all events (i.e., 3 MPa). In this way, we obtain a second set of slips that we consider representative of a homogeneous crustal mechanical condition, D_h. Therefore, for each 3-km along-strike bin, we cumulate the D and D_h values and compute the ratio of the two values. This ratio gives thus insights on a slip excess or deficit between the recorded seismicity properties and the ideal case with all earthquakes sharing the same rupture dynamic (i.e., the same $\Delta\sigma$). Further details can be found in Picozzi et al. (2022a). RSF along strike broadly shows high values over both segments of Cervialto and Marzano while it decreases crossing the Sele Valley that separates the two segments.

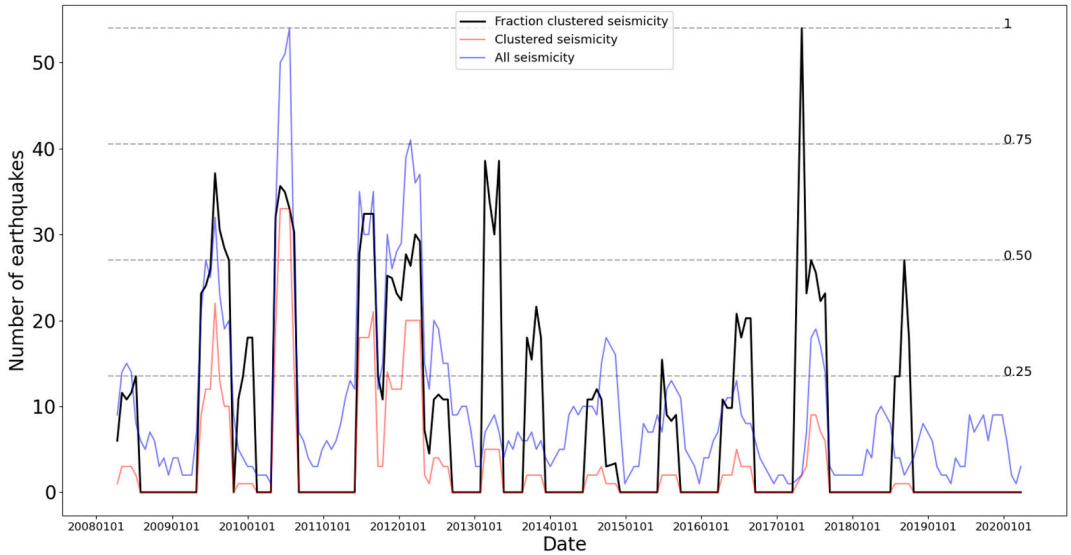

Fig. 5. Density of the whole seismicity used in this study and of the clustered seismicity over time.

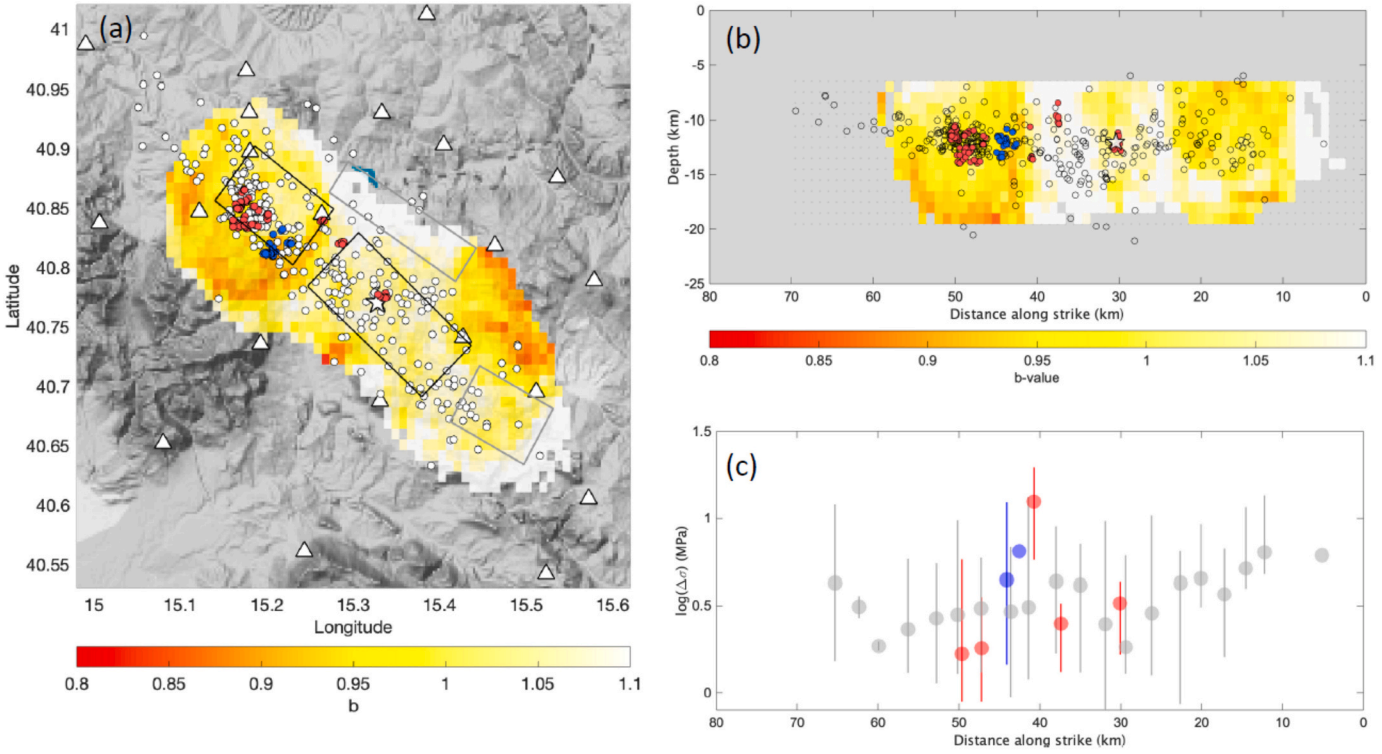

Fig. 6. (a) Positions of the clustered seismicity (red dots: earthquakes of C1 domain; blue dots: earthquakes of C2 domain) overlapped on the map of the b-value (redrawn from Picozzi et al., 2022a); (b) as in (a), but along the NW-SE profile. (c) Stress drop (values from Picozzi et al. (2022a)) averaged over distance bins along the strike with their standard deviation (vertical lines). Red, blue, gray dots mark respectively earthquakes of C1 domain, C2 domain, background seismicity. (For interpretation of the references to colour in this figure legend, the reader is referred to the web version of this article.)

Clustered seismicity mostly occurs in regions with Vp/Vs equal to 1.8 or lower, as inferred from previous tomographic studies (Amoroso et al., 2014; De Landro et al., 2022), which reveals also overall larger values of Vp/Vs in the volume of the Marzano segment (1.8–2) than in that of Cervialto segment (1.6–1.9) (Fig. S2). Apparently, the clustered seismicity of C2 domain nucleates within a patch with especially low Vp/Vs (1.75 or lower). An along-strike contrast in Vp/Vs is also confirmed by the application of the Wadati method (Wadati, 1928) on the differential travel times of two clusters (excluded in the definition of the clustered seismicity) crossing the Cervialto segment (Fig. S3). Although this approach has a lower spatial resolution than the tomography, it can be an independent estimate of Vp/Vs along the Cervialto segment. Similarly to the results of tomography, this approach shows that the northern part of the Cervialto segment has higher Vp/Vs than the lower part (Fig. S3), suggesting that C1 and C2 domains are characterized also by different Vp/Vs ratios.

Comparing the occurrence times of the earthquakes (clustered and nonclustered) and the nearly periodic deformation signal inferred from the GNSS recordings at the station of MCRV (Fig. 7), we observe a correlation between the clustered seismicity and the deformation. In particular, the clustered seismicity preferentially occurs in phases of large deformation of the karst aquifer, while it falls during periods of contraction. We highlight moreover that it is the clustered seismicity from domain C2 that shows the higher synchronization with the extreme values of the GNSS signal.

In line with these results, the Schuster test (Schuster, 1897; Petrosino et al., 2018 - Fig. S9) finds that the clustered seismicity is triggered at specific ranges of phases of a modulating cycle with a 1-year period, while the occurrence times of the background seismicity result distributed over a wider phase interval. The test however shows also that the phases of both clustered and background seismicity are unlikely generated by a purely random process, confirming that the earthquake rate in Irpinia has an overall imprinting of a cyclic phenomenon, which however appears more effective on the generation of the clustered seismicity.

4. Discussion

The first clear conclusion that can be inferred from the results of our study is that the two fault segments – Cervialto and Marzano – show very different tendency to produce clustered seismicity. In fact, although the number of earthquakes detected on the two segments is similar, almost half of the seismicity on the Cervialto segment belongs to the clustered seismicity, while this fraction for the Marzano segment is almost one tenth; most of the seismicity on this segment is thus diffused, except for two sequences occurred near the nucleation area of the 1980 EQ.

The spatial variability in the fraction of clustered seismicity has been proposed to be a proxy for inferring heterogeneity in fault coupling. For instance, Liu et al. (2022) investigated the seismicity along the San Andreas Fault (SAF) and found that the fraction of nonclustered seismicity is spatially correlated with aseismic slip, indicating that the creep rate along SAF is directly proportional to the fraction of nonclustered earthquakes. The presence of repeaters is also commonly interpreted as caused by cyclic stress accumulation and release on seismic patches in a creeping area (Uchida and Bürgmann, 2019). However, we do not have detailed enough geodetic information to speculate the existence of creep for the fault segments in the Irpinia area. In that sense, extending the earthquake catalog of the Irpinia fault network and therefore expanding the capability of detection of repeating earthquakes by machine-learning-based techniques (see Scotto di Uccio et al., 2023) could allow us to investigate this issue with the necessary resolution. The high variability of the fraction of clustered seismicity along strike (Fig. 8b) highlights that Cervialto and Marzano segments have different behavior, with a further peculiar and distinct way of behaving for the area named Sele Valley placed between the two segments. So, we can imagine three sectors with distinct properties. Both the variability of b-value and of

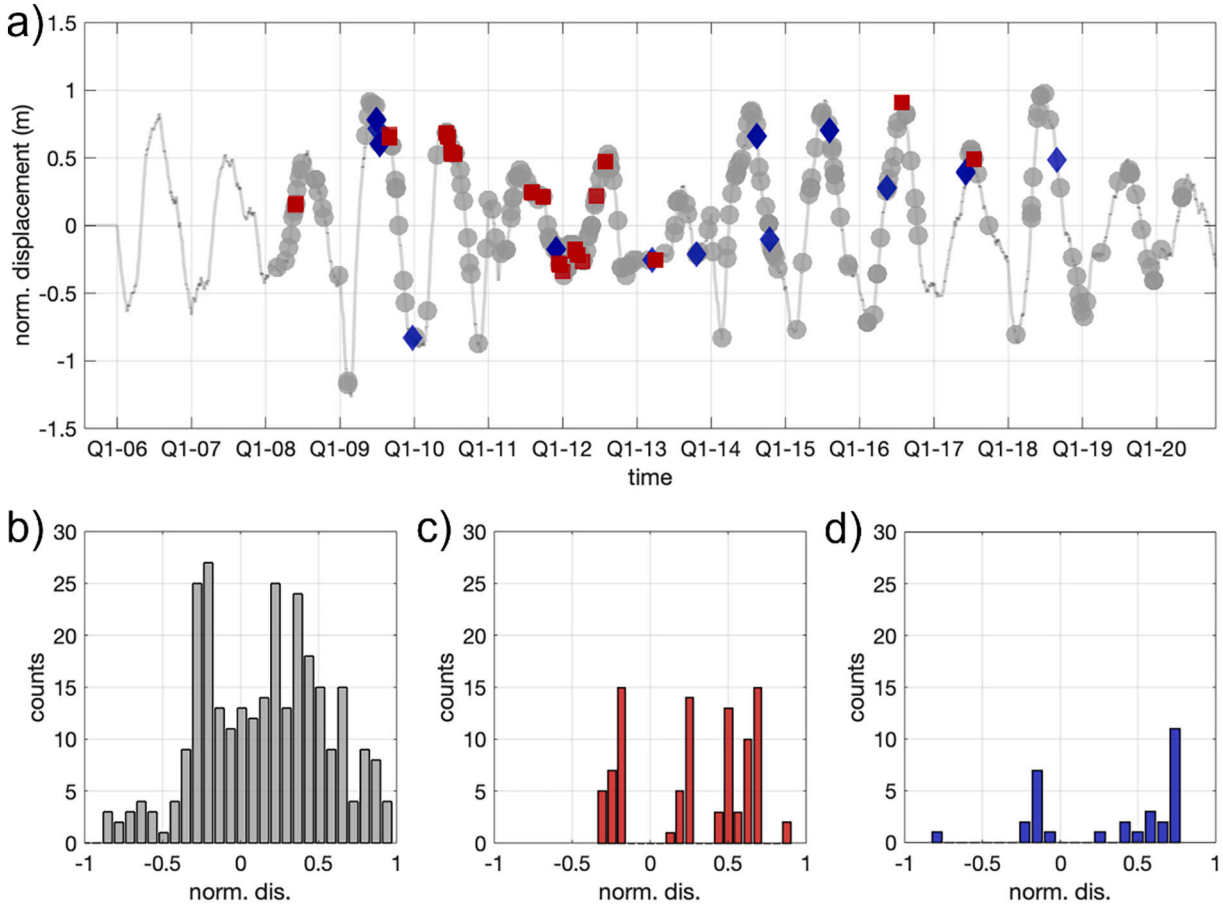

Fig. 7. GNSS signal (properly pre-processed and normalized) and occurrence times of the clustered seismicity (blue and red dots mark respectively occurrence times of earthquakes of C1 and C2 domain). b) Distribution of unclustered seismicity with respect to the GNSS signal. c) The same as b), but for the clustered seismicity C1. d) The same as b), but for the clustered seismicity C2. (For interpretation of the references to colour in this figure legend, the reader is referred to the web version of this article.)

RSF (Fig. 8a-b) along the average segment strike support our hypothesis.

The existence of this middle segment separating the Cervialto and Marzano segment is also confirmed by the cluster 17, which shows a dominant strike slip focal mechanism and along-dip is misaligned with the clusters 1–16 on the Cervialto segment (Fig. 3). The position of this cluster could mark the southern boundary of the Cervialto segment that in turn can spatially match a transcurrent fault, as proposed by Bello et al. (2021). In this framework, the transition between clusters 16 and 17 marks the transition between two fault segments and different fracturing mechanisms, with important implications for the seismic risk assessment: the Sele plain could act as a discontinuity in the rupture propagation, as indeed occurred also during the 1980 EQ (Bernard and Zollo, 1989; Pantosti and Valensise, 1990). Similarly, cluster 18, which shows a focal mechanism with a relevant strike-slip component and is aligned on the map with cluster 17 (Figs. 3, 4), could mark the southern boundary of the Sele plain edging the northern border of the Marzano segment.

Another important result of our work is the evidence that the clustered seismicity occurrence over time well matches the temporal evolution of deformation in karst aquifers (Fig. 7). In particular, the clustered seismicity of C2 domain shows a clear correlation with GNSS signals as the events mostly occur in correspondence of extreme values of the GPS recording; these extreme values correspond to the maximum carbonate deformation along the anti-Apennines direction (D'Agostino et al., 2018). This evidence suggests that the clustered seismicity can be activated also by a trigger mechanism where the anti-Apennine deformation of karst aquifer generates a stress increase which overlaps with the tectonic loading. The latter mechanism was originally proposed by D'Agostino et al. (2018). On the contrary, the rest of seismicity (background) does not appear to be clearly correlated to the GNSS signal.

All these results are compatible with a model in which the Cervialto and Marzano segments have different coupling values and, within the Cervialto segment, C1 and C2 domains show different frictional regimes and, in general, fracturing styles. In this framework, C2-domain has very high values of coupling and seismicity over this patch is only triggered for very high loading values. Moreover, the clustered seismicity of this domain is dominated by near-repeating earthquakes, whose existence is indeed in line with a high coupling fault interface (Uchida and Bürgmann, 2019). These earthquakes show uniformly overall on the C2-domain a normal fault mechanism, which matches the focal mechanisms of the main shock of 1980 EQ and confirms that all clusters of this domain are originated by the same rupture mechanism, although the locations show that the slipping may occur on multiple (two) subparallel faults (Figs. 3b, S4).

Considering C2 as a high-coupling subsegment, we calculate the cumulative slip generated by near-repeating events (Fig. S4), and we find that it ranges between ~1 cm and ~3 cm over a twelve-year period, which is compatible with the mean slip rate from geodetic information (i.e., ~3 mm/y; D'Agostino et al., 2018). Given the rather poor resolution of the geodetic measurements in the area, we can only compare in order of magnitude the two slip estimates; it cannot be thus excluded that a part of the slip would be aseismic, as indeed occurs in other seismic active areas generating repeating earthquakes (Uchida and Bürgmann, 2019).

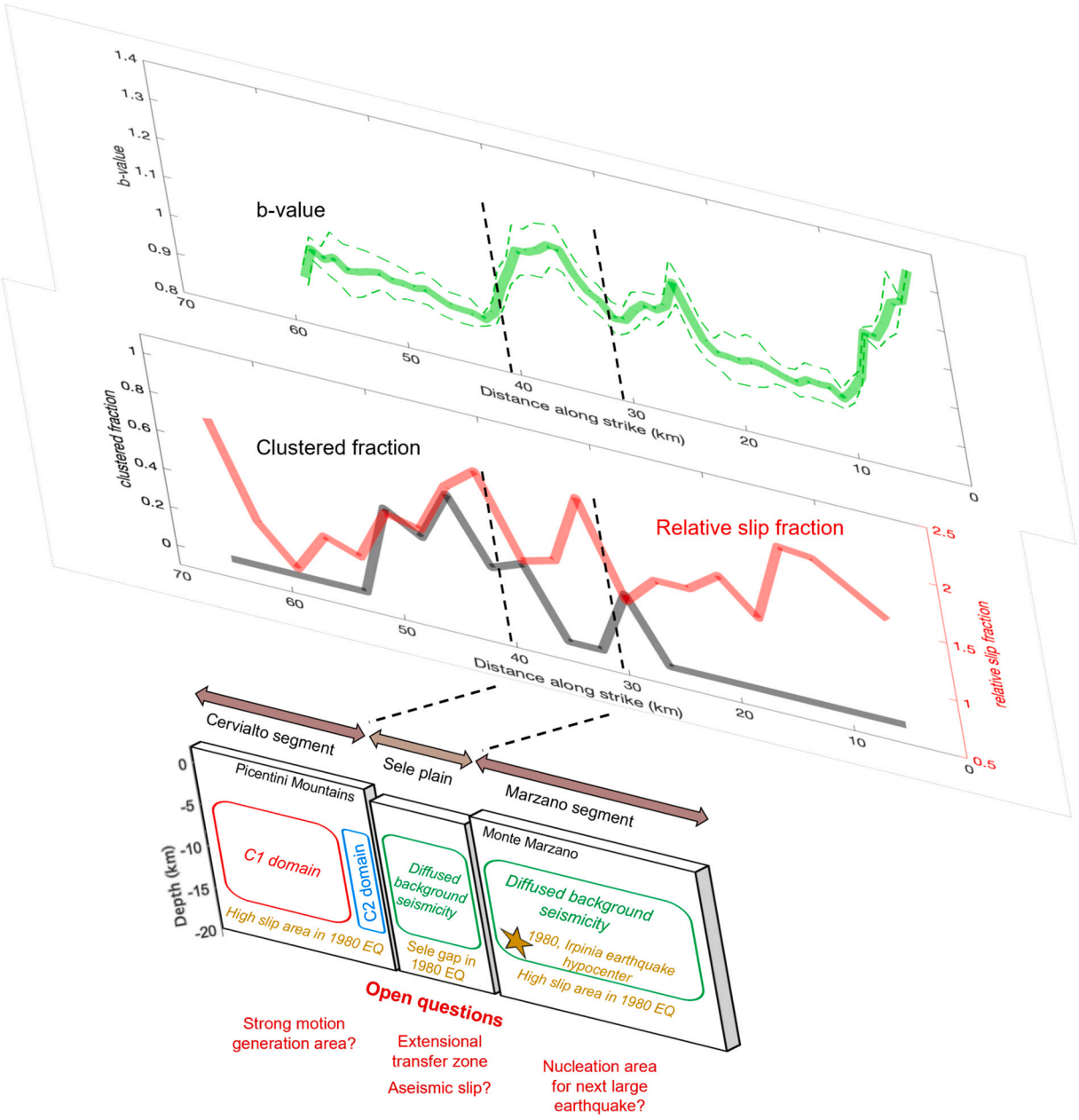

Fig. 8. a) b-values (from Picozzi et al. (2022a)) averaged over distance bins along the strike (solid yellow line) with their standard deviation (yellow dashed lines). Limits of the Sele river valley (vertical black dashed lines). b) The same as a), but showing the ratio of the clustered over the total (clustered + unclustered) seismicity (black line), and the relative slip fraction as red line. c) Outline of the Irpinia faults system with schematic representation of fault segments, a summary of main results and open questions concerning future hazard scenario. (For interpretation of the references to colour in this figure legend, the reader is referred to the web version of this article.)

Differently, the clustered seismicity in the C1-domain shows a more complex pattern of focal mechanisms with a combination of normal and strike-slip faulting. Similarly, the alignment of the hypocenters of the individual cluster do not depict a clear common fault plane (Fig. 3), suggesting a complex network of possibly interconnected small faults active in this domain.

A higher fault coupling in the C2-domain is also compatible with the higher values of the stress drop observed for the clustered seismicity in this subsegment than for the background seismicity. On the contrary, the clusters of C1 show on average lower stress drops. Overall, the seismicity of the Cervialto segment shows on average higher stress drops than those of the Marzano segment (Picozzi et al., 2022a).

An insight on the different stress conditions between the Cervialto and Marzano segments comes also from the contrast in the mean b-value and Vp/Vs ratio. The b-value appears overall smaller on the Cervialto than on the Marzano segment, with especially low values on the C2-domain (Fig. 6a,b). Similarly, the local Vp/Vs moves from 1.8–1.85 in the C1-domain to 1.7–1.75 in the C2 domain (Figs. S2, S3), indicating a potential contrast in the rheological properties of the two domains.

Based on all these elements, we try to sketch a model of the along-strike segmentation in the Cervialto-Marzano segments of the Irpinia fault network:

1. The Cervialto segment is characterized by clustered seismicity, relative low b-value and higher RSF. These features let us hypothesize that this segment presents high coupling (Fig. 8a,b). The latter aspect and the high capability to release higher ground motion intensity than the others (Picozzi et al., 2022a) let us consider this

segment as an asperity capable to potentially release high slip and to generate high strong motion during a future large event.
2. Within the Cervialto segment, the C1-domain hosts the clustered seismicity on a network of small faults with complex focal mechanisms. Moreover, this domain shows on average lower b-values and higher Vp/Vs ratios than the C2-domain, and the clustered seismicity is dominated by mainshock-aftershock sequences. We hypothesize for this domain an overall high coupling with a crucial role of the fluids in triggering the clustered (and maybe the whole) seismicity, as proposed also by Stabile et al. (2012) and by Scotto di Uccio et al. (2023). A possible small-scale fault network can promote the fluid flow.
3. Given the contrast in Vp/Vs and b-value between C1 and C2 and the predominance of near-repeaters in the C2-domain, we hypothesize for this subsegment a very high coupling and possibly a lower amount of fluids at depths of the considered seismicity. The clustered seismicity of this subsegment seems able to accommodate very efficiently the tectonic loading (and/or the loading of the aquifer) and thus can be potentially considered as a good proxy of the local strain.
4. The sector corresponding to the Sele Valley presents high b-value, which suggests the presence of fluids, high fraction of nonclustered seismicity and high RSF (Fig. 8). Reconstruction of the rupture evolution occurred during the 1980 EQ proposed a gap in slip for the Sele Valley (Cocco and Pacor, 1993). Further studies focused on this area are necessary to answer key questions: i) is this sector playing as extensional transfer zone?; ii) is this sector affected by aseismic slip?
5. The predominance of nonclustered seismicity suggests that the Marzano segment is characterized by a lower coupling than Cervialto. In the volume corresponding to the Marzano segment, that is in the same volume where the 1980 EQ nucleated, we observe today both relatively high b-values and RSF (Fig. 8). The high b-values are compatible with the existence of a porosity in carbonates around the 4–5% and a fluid composition consisting in brine-CO2 and/or CH4-CO2 found by Amoroso et al. (2014, 2017) by 3-D velocity images and rock physical modeling. Going further towards south, we note a progressive decrease of b-value and an increase in the RSF (Fig. 8).

Some authors (D'Agostino et al., 2018; De Landro et al., 2022; Picozzi et al., 2022b) have recently argued that the Irpinia fault network is close to a critical state because the intense seasonal rainfall (that recharges the shallow karst aquifer hosted in the carbonate Picentini Mountains and can lead to poroelastic deformation) is able to modulate deeper microseismicity. Here, we show an especially strong correlation between the clustered seismicity and the recharge of the karst aquifer, confirming that this seismicity is a very good proxy of the local stress conditions and suggesting that faults are critically stressed and easily influenced by hydrological forcing. Likely, their behavior is also influenced by high-pressure CO2 rich fluids identified in this area (Chiodini et al., 2010; Improta et al., 2014). Moreover, the high correlation between the recharge and the clustered seismicity of C2 suggests that this domain is particularly close to critical conditions.

Recent studies have observed both in the field and in laboratory that large earthquakes are sometimes preceded by a preparatory phase where a stable and slow rupture growth develops into an unstable rupture within a confined zone around the future hypocenter (Schurr et al., 2014; Socquet et al., 2017; Tape et al., 2018). Marzano, with all its characteristics, attracts our attention. Indeed, it shows temporal dependencies in its properties (Picozzi et al., 2019, 2022a, 2022b), lower coupling, high capability to promote slip, and at the same time in its southern part it results associated to high stress (i.e., low b-value, Scholz (2015), Fig. 8). These observations might be consistent with the development of a preparation phase, pushing us to pay particular attention to the future spatiotemporal evolution of microseismicity in this area.

CRediT authorship contribution statement

Mauro Palo: Conceptualization, Formal analysis, Methodology, Investigation, Software, Visualization, Writing – original draft, Writing – review & editing. **Matteo Picozzi:** Conceptualization, Writing – original draft, Data curation, Investigation, Writing – review & editing. **Grazia De Landro:** Formal analysis, Writing – review & editing, Software, Visualization. **Aldo Zollo:** Resources, Data curation, Writing – review & editing.

Declaration of Competing Interest

None.

Data availability

Data will be made available on request.

Acknowledgments

The research has been partially supported by the projects "FLUIDS - Detection and tracking of crustal fluid by multi-parametric methodologies and technologies" funded under the Italian PRIN-MUR programme (Grant no. 20174X3P29) and by the project "RETURN - multi-Risk sciEnce for resilienT commUnities undeR a changing climate" funded under the National Recovery and Resilience Plan (NRRP), Mission 4 Component 2 Investment 1.3 (Project code PE00000005). Data analysed in this work have been acquired by the ISNet (http://isnet.unina.it/) and are freely downloadable (www.ingv.it). Data processing has been partially performed using Python package Obspy (Beyreuther M., Barsch R., Krischer L., Megies T., Behr Y., Wassermann J., Obspy: a python toolbox for seismology Seismol. Res. Lett. 2010 530-533). Some maps have been plotted using Generic Mapping Tools (GMT ver.4; https://www.soest.hawaii.edu/gmt/, Wessel P., Smith W.H., New version of the generic mapping tools EOS Trans. Am. Geophys. Union 1995 329).

Appendix

Clustering

The starting point for the clustering of the earthquakes of the catalog is the definition of the cross-correlation (CC) matrix at each station. Each element of the CC matrix at one station contains the maximum of the CC function calculated between a pair of earthquakes detected at the station. For each earthquake pair i, j the CC function is calculated between signals of the vertical component of the velocimeters (or time-integrated accelerometers) filtered in the frequency range 1–20 Hz with a Butterworth digital filter of 4-th order, windowed with a box car with limits −0.4 s:+1 s (from the manually picked P arrival time) and tapered with a Tukey window (alpha factor: 0.4). On each one-station CC matrix, a Hierarchical Agglomerative Clustering (HAC) is applied to label each earthquake detected at a station with a one-station cluster index.

HAC is an unsupervised machine learning technique, in which the number of clusters is not fixed a priori. In this technique, the (dis)similarity matrix between the events is the input. In our case, they are the one-station CC matrices. Step by step, HAC amalgamates similar events and substitutes thus the merged events with a new "node". At each step, the (dis)similarity matrix is updated following a clustering strategy; we use the Ward's method (Gordon, 1987). Initially, all events are clusters with size 1; the merging ends up with all events belonging to one big cluster. The user stops the merging at a certain step by fixing the threshold of the largest dissimilarity between the events of a cluster, fixing in this way also the number of processes. We fix the threshold as the largest distance between fused objects among all merging steps, as proposed by Rowe et al. (2002).

Starting from the one-station CC matrices, a new "multi-channel"

matrix (MCM) is constructed, whose size equals the number of earthquakes in the catalog and that measures pairwise the similarity between the earthquakes. Each element *i,j* of MCM contains the maximum of the one-station CC value between the earthquake pair *i,j* over the stations detecting the pair.

If both earthquakes of the pair *i,j* are not detected at any common station, an estimation of the similarity between these two earthquakes is obtained in the following way. If event *i* is detected at stations A, B and event *j* at stations C, D, the union between the earthquakes belonging to the same one-station cluster of event *i* detected at station A and the earthquakes belonging to the same one-station cluster of event *i* detected at station B is performed (U_i). These earthquakes can be assumed to be very similar in waveform to the event *i* at stations A and B. They are then sorted by the CC value with event *i* (for each pair $i - U_i$ the channel with the highest CC is considered). The same procedure is repeated for event *j* with stations C and D. The set of earthquakes similar to event *j* in this case is indicated as U_j, whose elements are then sorted by their CC value with event *j*, as well. Among all earthquakes detected at station A only those contained in the set U_j are considered; we call this subset $U_{j,A}$. The events of this subset can be considered a good representation of event *j* at station A, where actually it was not detected. The average of the CCs between event *i* and those of $U_{j,A}$ is the inference of the similarity between events *i* and *j* at stations A. If $U_{j,A}$ has more than ten events, the rest is discarded in the average to assure to consider only earthquakes very similar in waveforms with event *j* (U_j is sorted by CC with event *j*). Similarly, $U_{j,B}$ is defined and the similarity between events *i* and *j* at stations B is calculated. The same procedure is repeated intersecting all earthquakes detected at station C (D) with those contained in the set U_i, inferring thus an imputation of the similarity between events *i* and *j* at station C (D). The final value of the similarity between events *i* and *j* is eventually the maximum among the similarities at the four stations. In case $U_{i/j,A-D}$ are all empty, it is assumed that events *i* and *j* are totally dissimilar. In this way, a "multi-channel" similarity matrix MCM can be defined, whose elements measure the similarity between two earthquakes, estimating the similarity even between those not detected at any common stations. HAC is then applied to MCM (with the same setting used to calculate the one-station cluster indices), and a final cluster index is eventually assigned to each earthquake of the catalog. MCC thus performs a two-level HAC, one on the one-station CC matrices, another on the MCM, by which we provide a cluster label for each earthquake of the catalog. However, to ensure that only earthquakes with real similar waveforms are collected into a family, among all clusters we select those whose CC median at least at one station is higher than 0.7 calculated on four events or more (so doublets are discarded). The earthquakes composing these clusters constitute the clustered seismicity. Earthquakes not included in these clusters are defined as composing the background seismicity.

Appendix A. Supplementary data

Supplementary data to this article can be found online at https://doi.org/10.1016/j.tecto.2023.229849.

References

Aki, K., 1965. Maximum likelihood estimate of b in the formula logn= a-bm and its confidence limits. Bull. Earthq. Res. Inst., Univ. Tokyo 43, 237–239.

Amoroso, O., Ascione, A., Mazzoli, S., Virieux, J., Zollo, A., 2014. Seismic imaging of a fluid storage in the actively extending Apennine mountain belt, southern Italy. Geophys. Res. Lett. 41 (11), 3802–3809.

Amoroso, O., Russo, G., De Landro, G., Zollo, A., Garambois, S., Mazzoli, S., Parente, M., Virieux, J., 2017. From velocity and attenuation tomography to rock physical modeling: Inferences on fluid-driven earthquake processes at the Irpinia fault system in southern Italy. Geophys. Res. Lett. 44 (13), 6752–6760.

Avouac, J.P., 2015. From geodetic imaging of seismic and aseismic fault slip to dynamic modeling of the seismic cycle. Annu. Rev. Earth Planet. Sci. 43, 233–271.

Barchi, M., 1998. The crop 03 profile: a synthesis of results on deep structures of the northern Apennines. Mem. Soc. Geol. It. 52, 383–400.

Bello, S., De Nardis, R., Scarpa, R., Brozzetti, F., Cirillo, D., Ferrarini, F., Di Lieto, B., Arrowsmith, R.J., Lavecchia, G., 2021. Fault pattern and seismotectonic style of the Campania–Lucania 1980 earthquake (mw 6.9, southern Italy): new multidisciplinary constraints. Front. Earth Sci. 8, 608063.

Bernard, P., Zollo, A., 1989. The Irpinia (Italy) 1980 earthquake: detailed analysis of a complex normal faulting. J. Geophys. Res. 94 (B2), 1631–1647.

Bilek, S.L., Lay, T., 2002. Tsunami earthquakes possibly widespread manifestations of frictional conditional stability. Geophys. Res. Lett. 29 (14), 18–1.

Brune, J.N., 1970. Tectonic stress and the spectra of seismic shear waves from earthquakes. J. Geophys. Res. 75 (26), 4997–5009.

Castro, R., Anderson, J., Singh, S., 1990. Site response, attenuation and source spectra of s waves along the Guerrero, Mexico, subduction zone. Bull. Seismol. Soc. Am. 80 (6A), 1481–1503.

Chiarabba, C., Amato, A., 2003. eVp and Vp/Vs images in the Mw 6.0 Colfiorito fault region (central Italy): a contribution to the understanding of seismotectonic and seismogenic processes. J. Geophys. Res. Solid Earth 108 (B5).

Chiarabba, C., De Gori, P., Cattaneo, M., Spallarossa, D., Segou, M., 2018. Faults geometry and the role of fluids in the 2016–2017 central Italy seismic sequence. Geophys. Res. Lett. 45 (14), 6963–6971.

Chiodini, G., Granieri, D., Avino, R., Caliro, S., Costa, A., Minopoli, C., Vilardo, G., 2010. Non-volcanic CO2 earth degassing: case of Mefite d'ansanto (Southern Apennines), Italy. Geophys. Res. Lett. 37 (11).

Cocco, M., Pacor, F., 1993. The rupture process of the 1980 Irpinia, Italy, earthquake from the inversion of strong motion waveforms. Tectonophysics 218 (1–3), 157–177.

D'Agostino, N., Silverii, F., Amoroso, O., Convertito, V., Fiorillo, F., Ventafridda, G., Zollo, A., 2018. Crustal deformation and seismicity modulated by groundwater recharge of karst aquifers. Geophys. Res. Lett. 45(22):12,253–12,262.

De Landro, G., Amoroso, O., Alfredo Stabile, T., Matrullo, E., Lomax, A., Zollo, A., 2015. High-precision differential earthquake location in 3-D models: evidence for a rheological barrier controlling the microseismicity at the Irpinia fault zone in southern Apennines. Geophys. J. Int. 203 (3), 1821–1831.

De Landro, G., Amoroso, O., Russo, G., D'Agostino, N., Esposito, R., Emolo, A., Zollo, A., 2022. Decade-long monitoring of seismic velocity changes at the Irpinia fault system (southern Italy) reveals pore pressure pulsations. Sci. Rep. 12 (1), 1247.

Di Luccio, F., Ventura, G., Di Giovambattista, R., Piscini, A., Cinti, F., 2010. Normal faults and thrusts reactivated by deep fluids: The 6 april 2009 Mw 6.3 L'Aquila earthquake, central Italy. J. Geophys. Res. Solid Earth 115 (B6).

Doetsch, J., Gischig, V.S., Villiger, L., Krietsch, H., Nejati, M., Amann, F., Jalali, M., Madonna, C., Maurer, H., Wiemer, S., et al., 2018. Subsurface fluid pressure and rock deformation monitoring using seismic velocity observations. Geophys. Res. Lett. 45 (19), 10–389.

Doglioni, C., Barba, S., Carminati, E., Riguzzi, F., 2014. Fault on–off versus coseismic fluids reaction. Geosci. Front. 5 (6), 767–780.

Efron, B., 2000. The bootstrap and modern statistics. J. Am. Stat. Assoc. 95 (452), 1293–1296.

Festa, G., Adinolfi, G.M., Caruso, A., Colombelli, S., De Landro, G., Elia, L., Emolo, A., Picozzi, M., Scala, A., Carotenuto, F., Gammaldi, S., Iaccarino, A.G., Nazeri, S., Riccio, R., Russo, G., Tarantino, S., Zollo, A., 2021. Insights into mechanical properties of the 1980 Irpinia fault system from the analysis of a seismic sequence. Geosciences (Switzerland) 11 (1), 1–24.

Gentili, S., Di Giovambattista, R., 2017. Pattern recognition approach to the subsequent event of damaging earthquakes in Italy. Phys. Earth Planet. Inter. 266, 1–17.

Gordon, A.D., 1987. A review of hierarchical classification. J. Roy. Stat. Soc. Ser. A (General) 150 (2), 119.

Gutenberg, B., Richter, C.F., 1942. Earthquake magnitude, intensity, energy, and acceleration. Bull. Seismol. Soc. Am. 32 (3), 163–191.

Herrmann, M., Piegari, E., Marzocchi, W., 2022. Revealing the spatiotemporal complexity of the magnitude distribution and b-value during an earthquake sequence. Nat. Commun. 13 (1), 1–10.

Hotovec-Ellis, A.J., Jeffries, C., 2016. Near Real-Time Detection, Clustering, and Analysis of Repeating Earthquakes: Application to Mount St. Helens and Redoubt Volcanoes. Available at: https://github.com/ahotovec/REDPy.

Iannaccone, G., Zollo, A., Elia, L., Convertito, V., Satriano, C., Martino, C., Festa, G., Lancieri, M., Bobbio, A., Stabile, T.A., Vassallo, M., Emolo, A., 2010. A prototype system for earthquake early-warning and alert management in southern Italy. Bull. Earthq. Eng. 8 (5), 1105–1129.

Improta, L., De Gori, P., Chiarabba, C., 2014. New insights into crustal structure, Cenozoic magmatism, CO2 degassing, and seismogenesis in the southern Apennines and Irpinia region from local earthquake tomography. J. Geophys. Res. Solid Earth 119 (11), 8283–8311.

Johnson, K.M., 2006. Frictional properties on the San Andreas fault near Parkfield, California, inferred from models of afterslip following the 2004 earthquake. Bull. Seismol. Soc. Am. 96, S321–S338.

Kanamori, H., Heaton, T.H., Rundle, J., 2000. Microscopic and macroscopic physics of earthquakes. Geophysical Monograph-American Geophysical Union 120, 147–164.

Lay, T., Kanamori, H., 1981. An asperity model of large earthquake sequences. Earthq. Prediction Int. Rev. 4, 579–592.

Lay, T., Kanamori, H., Ammon, C.J., Koper, K.D., Hutko, A.R., Ye, L., Yue, H., Rushing, T. M., 2012. Depth-varying rupture properties of subduction zone megathrust faults. J. Geophys. Res. Solid Earth 117 (B4).

Liu, Y.-K., Ross, Z.E., Cochran, E.S., Lapusta, N., 2022. A unified perspective of seismicity and fault coupling along the San Andreas fault. Sci. Adv. 8 (8) eabk1167.

Lomax, A., Michelini, A., Curtis, A., 2009. Earthquake location, direct, global-search methods. Encyclopedia of Complexity and Systems Science, pp. 2449–2473.

Manighetti, I., Campillo, M., Bouley, S., Cotton, F., 2007. Earthquake scaling, fault segmentation, and structural maturity. Earth Planet. Sci. Lett. 253 (3–4), 429–438.

Matrullo, E., De Matteis, R., Satriano, C., Amoroso, O., Zollo, A., 2013. An improved 1-d seismic velocity model for seismological studies in the Campania–Lucania region (southern Italy). Geophys. J. Int. 195 (1), 460–473.
Moreno, M., Melnick, D., Rosenau, M., Baez, J., Klotz, J., Oncken, O., Tassara, A., Chen, J., Bataille, K., Bevis, M., Socquet, A., Bolte, J., Vigny, C., Brooks, B., Ryder, I., Grund, V., Smalley, B., Carrizo, D., Bartsch, M., Hase, H., 2012. Toward understanding tectonic control on the Mw 8.8 2010 Maule Chile earthquake. Earth Planet. Sci. Lett. 321-322, 152–165.
Niemeijer, A.R., Vissers, R.L.M., 2014. Earthquake rupture propagation inferred from the spatial distribution of fault rock frictional properties. Earth Planet. Sci. Lett. 396, 154–164.
Pantosti, D., Valensise, G., 1990. Faulting mechanism and complexity of the November 23, 1980, Campania-Lucania earthquake, inferred from surface observations. J. Geophys. Res. 95 (B10), 15319.
Pantosti, D., Valensise, G., 1993. Source geometry and long term behavior of the 1980, Irpinia earthquake fault based on field geologic observations. Ann. Geophys. 36 (1).
Petrosino, S., Cusano, P., Madonia, P., 2018. Tidal and hydrological periodicities of seismicity reveal new risk scenarios at Campi Flegrei caldera. Sci. Rep. 8 (1), 1–12. https://doi.org/10.1038/s41598-018-31760-4.
Picozzi, M., Oth, A., Parolai, S., Bindi, D., De Landro, G., Amoroso, O., 2017. Accurate estimation of seismic source parameters of induced seismicity by a combined approach of generalized inversion and genetic algorithm: application to the geysers geothermal area, California. J. Geophys. Res. Solid Earth 122 (5), 3916–3933.
Picozzi, M., Bindi, D., Zollo, A., Festa, G., Spallarossa, D., 2019. Detecting long-lasting transients of earthquake activity on a fault system by monitoring apparent stress, ground motion and clustering. Sci. Rep. 9 (1).
Picozzi, M., Bindi, D., Festa, G., Cotton, F., Scala, A., D'Agostino, N., 2022a. Spatiotemporal evolution of microseismicity seismic source properties at the Irpinia Near-Fault Observatory, Southern Italy. Bull. Seismol. Soc. Am. 112 (1), 226–242.
Picozzi, M., Cotton, F., Bindi, D., Emolo, A., Maria Adinolfi, G., Spallarossa, D., Zollo, A., 2022b. Spatiotemporal evolution of ground-motion intensity at the Irpinia Near-Fault Observatory, Southern Italy. Bull. Seismol. Soc. Am. 112 (1), 243–261.
Picozzi, M., Spallarossa, D., Bindi, D., Iaccarino, A.G., Rivalta, E., 2022c. Detection of spatial and temporal stress changes during the 2016 central Italy seismic sequence by monitoring the evolution of the energy index. Journal of Geophysical Research: Solid Earth 127 (11) e2022JB025100.
Picozzi, M., Spallarossa, D., Iaccarino, A., Bindi, D., 2022d. Temporal evolution of radiated energy to seismic moment scaling during the preparatory phase of the Mw 6.1, 2009 L'Aquila earthquake (Italy). Geophys. Res. Lett. 49 (8) e2021GL097382.
Reasenberg, P.A., 1985. FPFIT, FPPLOT, and FPPAGE: Fortran computer programs for calculating and displaying earthquake fault-plane solutions. US Geol. Surv. Open-File Rep., pp. 85–739.
Rowe, C.A., Aster, R.C., Borchers, B., Young, C.J., 2002. An automatic, adaptive algorithm for refining phase picks in large seismic data sets. Bull. Seismol. Soc. Am. 92 (5), 1660–1674.
Scholz, C.H., 2015. On the stress dependence of the earthquake b value. Geophys. Res. Lett. 42 (5), 1399–1402.
Schurr, B., Asch, G., Hainzl, S., Bedford, J., Hoechner, A., Palo, M., Wang, R., Moreno, M., Bartsch, M., Zhang, Y., Oncken, O., Tilmann, F., Dahm, T., Victor, P., Barrientos, S., Vilotte, J.P., 2014. Gradual unlocking of plate boundary controlled initiation of the 2014 Iquique earthquake. Nature 512, 299–302.
Schuster, Arthur, 1897. On lunar and solar periodicities of earthquakes. Proc. R. Soc. Lond. 61 (369–377), 455–465.
Scotto di Uccio, F., Scala, A., Festa, G., Picozzi, M., Beroza, G.C., May 2023. Comparing and integrating artificial intelligence and similarity search detection techniques: application to seismic sequences in Southern Italy. Geophys. J. Int. 233 (2), 861–874.
Shearer, P., Hauksson, E., Lin, G., 2005. Southern California hypocenter relocation with waveform cross-correlation, part 2: results using source-specific station terms and cluster analysis. Bull. Seismol. Soc. Am. 95 (3), 904–915. https://doi.org/10.1785/0120040168.
Shelly, D.R., Ellsworth, W.L., Hill, D.P., 2016. Fluid-faulting evolution in high definition: Connecting fault structure and frequency-magnitude variations during the 2014 Long Valley Caldera, California, earthquake swarm. J. Geophys. Res. 121 (3), 1776–1795.
Socquet, A., Valdes, J.P., Jara, J., Cotton, F., Walpersdorf, A., Cotte, N., Specht, S., Ortega-Culaciati, F., Carrizo, D., Norabuena, E., 2017. An 8 month slow slip event triggers progressive nucleation of the 2014 Chile megathrust. Geophys. Res. Lett. 44 (9), 4046–4053.
Stabile, T.A., Satriano, C., Orefice, A., Festa, G., Zollo, A., 2012. Anatomy of a microearthquake sequence on an active normal fault. Sci. Rep. 2.
Tape, C., Holtkamp, S., Silwal, V., Hawthorne, J., Kaneko, Y., Ampuero, J.P., Ji, C., Ruppert, N., Smith, K., West, M.E., 2018. Earthquake nucleation and fault slip complexity in the lower crust of Central Alaska. Nat. Geosci. 11 (7), 536–541.
Trugman, D.T., Shearer, P.M., 2017. GrowClust: a hierarchical clustering algorithm for relative earthquake relocation, with application to the Spanish Springs and Sheldon, Nevada, earthquake sequences. Seismol. Res. Lett. 88 (2), 379–391. https://doi.org/10.1785/0220160188.
Uchida, N., Bürgmann, R., 2019. Repeating Earthquakes. Annu. Rev. Earth Planet. 47, 305–332.
Valensise, G., Pantosti, D., 2001. The investigation of potential earthquake sources in peninsular Italy: a review. J. Seismol. 5 (3), 287–306.
Vuan, A., Sugan, M., Amati, G., Kato, A., 2018. Improving the detection of low-magnitude seismicity preceding the Mw 6.3 L'Aquila earthquake: Development of a scalable code based on the cross correlation of template earthquakes. Bull. Seismol. Soc. Am. 108 (1), 471–480.
Wadati, K., 1928. Shallow and deep earthquakes. Geophys. Mag. 1, 162–202.
Waldhauser, F., Ellsworth, W.L., 2000. A double-difference earthquake location algorithm: method and application to the Northern Hayward Fault, California. Bull. Seismol. Soc. Am. 90 (6), 1353–1368.
Wang, C., Wu, J., He, X., Ye, M., Liu, W., Tang, R., 2019. Emerging trends and new developments in disaster research after the 2008 Wenchuan earthquake. Int. J. Environ. Res. Public Health 16 (1), 29.
Weber, E., Iannaccone, G., Zollo, A., Bobbio, A., Cantore, L., Corciulo, M., Convertito, V., Crosta, M.D., Elia, L., Emolo, A., et al., 2007. Development and testing of an advanced monitoring infrastructure (ISNET) for seismic early-warning applications in the Campania region of southern Italy. In: Earthquake Early Warning Systems. Springer, pp. 325–341.
Westaway, R., Jackson, J., 1987. The earthquake of 1980 November 23 in Campania—Basilicata (southern Italy). Geophys. J. Int. 90 (2), 375–443.
Wiemer, S., 2001. A software package to analyze seismicity: ZMAP. Seismol. Res. Lett. 72 (3), 373–382.